Journal of Solid State Chemistry **147,** 92–98 (1999)
Article ID jssc.1999.8182, available online at http://www.idealibrary.com on IDEAL®

# Synthesis and *ab Initio* Structure Determination from X-Ray Powder Diffraction of MIL-12, a New Layered Fluoroaluminophosphate Templated with 1,3 Diaminopropane: $[N_2C_3H_{12}]Al_2(PO_4)(OH_x, F_{5-x})$ ($x \approx 2$)

N. Simon,* N. Guillou,* T. Loiseau,* F. Taulelle,† and G. Férey*

*Institut Lavoisier UMR CNRS 173, Université de Versailles-St Quentin en Yvelines, 45 avenue des Etats Unis, 78035 Versailles cedex, France; and †RMN et Chimie du solide, UMR 7510 ULP-Bruker-CNRS, Université Louis Pasteur, 4 rue Blaise Pascal, 67070 Strasbourg cedex, France

Received October 12, 1998; accepted January 22, 1999

DEDICATED TO PROFESSOR JEAN ROUXEL

**MIL-12, formulated $Al_2(PO_4)(OH_x, F_{5-x})N_2C_3H_{12}$, with $x \approx 2$, is a new layered fluoroaluminophosphate formed at the early stages of ULM-4 by hydrothermal synthesis using 1-3, Diaminopropane as a template ($Al(OH)_3/H_3PO_4/HF$/1-3 DAP/$H_2O$ : ratio 1 : 1 : 3 : 0.5 : 80, 180°C/2 days). It crystallises in the monoclinic space group $P2_1/m$ with $a$=11.072(1) Å, $b$=7.012 (2) Å, $c$=6.1096 (8) Å, $\beta$=100.98 (1)° and $Z$=2. Its structure was solved *ab initio* from conventional X-ray powder diffraction data and refined by the Rietveld method with satisfactory crystal-structure model indicators ($R_B$=0.088 and $R_F$= 0.062) and profile factors ($R_{wp}$=0.124 and $R_p$=0.161). It consists of $[Al_2(PO_4)(OH, F)_5^{-2}]$ macroanionic sheets perpendicular to the $a$ axis in which $OH^-$ and $F^-$ ions are statistically distributed. Aluminum octahedra are linked together to form zig-zag chains running parallel to the $b$ axis; the phosphate groups ensure the connection of the aluminum chains within the (100) layer. Protonated 1-3, Diaminopropane is interleaved between the sheets and ensures the cohesion of the structure by hydrogen bonds. Structural relations with other solids built with the same type of chains are presented.** © 1999 Academic Press

## 1. INTRODUCTION

In 1982, Wilson *et al.* (1) reported a novel class of microporous aluminophosphate materials ($AlPO_4$-*n*). Some years later, Guth *et al.* (2) developed a new route of synthesis by adding fluorine to the starting mixture. Using this method, a new series of fluorometallophosphates, initially labelled ULM-*n* (for Université Le Mans) and then MIL-*n* (for Materials of Institute Lavoisier) has been prepared in the systems: *M*–*P*–*F*–amine–$H_2O$ with *M* = Al, Ga, V, Fe, and Ti (3–7). The numerous structure types of the microporous compounds of this series demonstrate the influence of the templating agent as well as fluorine during the synthesis and allow for the proposal of a mechanism of formation (8). It was recently shown that the ULM-4 structural type could be obtained with either gallium, aluminum, or iron (8–12). Moreover, the kinetic study of the crystallization of ULM-4 showed that a secondary phase was obtained at the beginning of its synthesis and that the amount of this new phase decreased slowly with the test duration for the benefit of ULM-4 (12). This unknown phase named MIL-12 and formulated $Al_2(PO_4)(OH_x, F_{5-x})N_2C_3H_{12}$, with $x \approx 2$, has been isolated as a pure phase by increasing the amount of fluorine. We present here its synthesis and its *ab initio* crystal structure determination from X-ray powder diffraction data.

## 2. EXPERIMENTAL

A first synthesis of MIL-12 was carried out hydrothermally in a 23-ml Teflon-lined Parr bomb under autogenous pressure. Aluminium hydroxide ($Al(OH)_3$, Prolabo R.P. Rectapur, 98%), phosphoric acid ($H_3PO_4$, Prolabo R.P. Normapur, 85%), fluorhydric acid (HF, Prolabo R.P. Normapur, 48%), 1,3 diaminopropane ($H_2N(CH_3)_3NH_2$, Aldrich, 99%), and distilled water were introduced without stirring successively in a teflon container in the molar ratio 1 : 1 : 3 : 0.5 : 80 with a filling rate of 20%, while the molar ratio of the ULM-4 synthesis is 1 : 1 : 1 : 0.5 : 80 for the same reactants. The bomb was then placed in an autoclave at 180°C for 96 h. The pH of the solution ( $\approx$ 2) was the same at the beginning and at the end of the reaction. The obtained crystalline product was filtered off, washed with distilled water, and dried at room temperature. The morphology of the crystals was characterized by scanning electron microscopy (JEOL JSM-5800 LV instrument, using accelerating voltage in the range of 15–20 kV). The title product was



0022-4596/99 $30.00

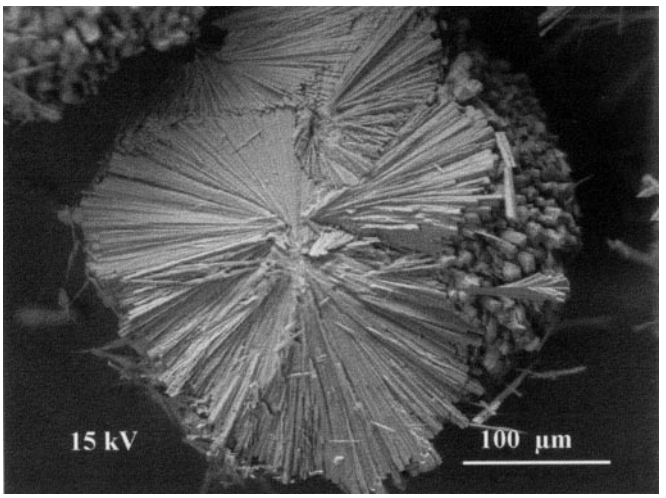


**FIG. 1.** Scanning electron micrograph of MIL-12.

obtained in a pure form and appears as very thin fibrous-like crystals stacked in spherical shape (Fig. 1). The too-small size of the crystals ruled out any single-crystal X-ray analysis. The X-ray powder pattern showed large preferred orientation effects. In order to avoid this effect, another synthesis was then carried out in a large Teflon vessel of 125 ml under stirring conditions for 2 days, keeping the same experimental conditions with the same molar ratio and filling rate. The resulting product was then a very fine, pure, and well-crystallized powder that could be easily characterized by X-ray powder diffraction.

The chemical analysis of the solid gave: Al 15.06; P 8.81; F 19.13; C 10.81; N 8.45 (wt. %). These results are in fair agreement with the theoretical values calculated for the chemical formula $Al_2(PO_4)(OH_x, F_{5-x})\ N_2C_3H_{12}$, with $x = 2$ ($\%_{th}$: Al 17.07; P 9.80; F 18.03; C 11.40; N 8.86). X-ray diffraction results confirmed the Al, P, and amine composition.

The thermogravimetric analysis of MIL-12 was performed on a TA-instrument type 2050 thermoanalyzer under nitrogen gas flow with a heating rate of $5^\circ\ mn^{-1}$ between 50° and 600°C. The thermogram revealed a unique weight loss of 35.8% (th. 35.5%) above 250°C (Fig. 2). The final residue at 600°C is polyphasic and the only crystalline part was $AlF_3$, besides, an amorphous product.

The X-ray powder diffraction data were collected on a Siemens D5000 diffractometer using Cu$K\alpha$ radiation ($\lambda = 1.5418$ Å). To minimize preferred orientation effects, the powder was side loaded. The powder diffraction pattern was scanned over the angular range 6–100° ($2\theta$), with a step size of 0.02° ($2\theta$). The counting times were 32 s $step^{-1}$ to 49.84° and 64 s $step^{-1}$ from 49.86° to the end of the scan, in order to improve the counting statistics of the high-angle region. The full pattern was then scaled to the lower counting time. The contribution of Cu$K\alpha_2$ radiation was removed from the pattern by means of the software package DIFFRACT-AT and an accurate determination of the peak positions and relative intensities for Cu$K\alpha_1$ radiation contribution was carried out. The pattern indexing was performed by means of the computer program DICVOL91 (13) from the twenty first lines, with an absolute error on peak positions of 0.03° ($2\theta$). A monoclinic solution was found with satisfactory figures of merit [$M_{20} = 77$ and $F_{20} = 138$ (0.0056, 26)]. From the complete data set, reviewed by means of the program NBS*AIDS83 (14), the refined cell parameters given in Table 1 were obtained [$M_{20} = 67$ and $F_{30} = 114$(0.069, 38)]. The powder diffraction data are reported in Table 2 for Cu$K\alpha_1$ radiation ($\lambda = 1.5406$ Å). Systematic absences ($0k0$, $k = 2n + 1$) were consistent with the two space groups $P2_1$ and $P2_1/m$.

Integrated intensities in the angular range 6–80° ($2\theta$) were extracted using FULLPROF program (15). Calculations were performed with the SIRPOW92 program (16). The centrosymmetric space group $P2_1/m$ was chosen to solve the structure. Direct Methods and Fourier calculations provided the location at all nonhydrogen atoms, which were refined by the Rietveld method. A pseudo-Voigt function was selected to describe individual line profiles. In order to describe the angular dependence of the peak fullwidth at half maximum, the usual quadratic function in $\tan\theta$ was used. Five regions of the powder pattern were excluded due to the presence of spurius diffraction lines of the sample holder. The final Rietveld refinement using 959 Fobs was carried out in the angular range 6–96° ($2\theta$). Figure 3 shows the final fit obtained between calculated and observed patterns. It corresponds to satisfactory crystal structure model indicators ($R_F = 0.062$ and $R_B = 0.088$) and profile factors ($R_p = 0.124$ and $R_{wp} = 0.161$). Details to the refinement are

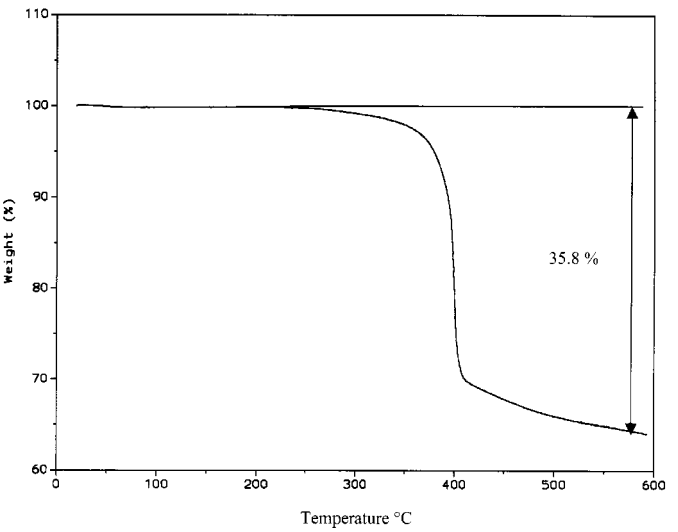


**FIG. 2.** Thermogravimetric analysis of MIL-12 under Nitrogen atmosphere (heating rate 5°C $min^{-1}$).

**TABLE 1**
**Crystallographic Data for $(C_3H_{12}N_2)Al_2PO_4(OH,F)_5$**

| | |
|---|---|
| Chemical formula weight (g mol$^{-1}$) | 316.085 |
| Calculated density (g cm$^{-3}$) | 2.255 |
| Experimental density (g cm$^{-3}$) | 2.252(8) |
| Crystal system | Monoclinic |
| Space group | $P2_1/m$ |
| $a$ (Å) | 11.072(1) |
| $b$ (Å) | 7.012(1) |
| $c$ (Å) | 6.1096(8) |
| $\beta$ (°) | 100.98(1) |
| $V$ (Å$^3$) | 465.62(8) |
| Figures of merit | $M_{20}=67$; $F_{30}=114(0.0069, 38)$ |
| $Z$ | 2 |
| Radiation (Å) | 1.5418 |
| $2\theta$ range (°) | 6–96 |
| Number of reflections | 959 |
| Number of atoms | 14 |
| Number of structural parameters | 31 |
| $R_P$ | 0.124 |
| $R_{WP}$ | 0.161 |
| $R_B$ | 0.088 |
| $R_F$ | 0.062 |

summarized in Table 1. Final atomic parameters are given in Table 3. Selected bond distances and angles are listed in Table 4.

Moreover, with powder X-ray diffraction, it should be noted that oxygen, fluorine, or hydroxyl groups cannot be easily distinguished. So, the final refinement of MIL-12 has been made with oxygen groups on the following sites: (OH, F) 1, (OH, F)2, and (OH, F)3.

The nuclear magnetic resonance experiment was recorded with a Bruker DSX500 spectrometer. The $^{19}F$ spectrum was acquired at a spinning rate of 30 kHz (2.5 mm rotor) under the following conditions: $^1H$ nondecoupling; $\pi/2$ pulse length = 4 μs; dead time = 4.5 μs; pulse delay (recycle time) = 30 s; resonance frequency = 470.6 MHz; number at scans = 256; number of digitized points = 8 kwords; referencing 0 ppm: $CFCl_3$. The $^{19}F$ MAS spectrum (Fig. 4) reveals a broad resonnance signal around − 140 ppm. This chemical shift value is that expected for the Al–F bonding as already found in the aluminophosphate $AlPO_4$–CJ2 (17). The peak can be decomposed as a sum of four Lorentzian–Gaussian lines (Winfit program simulation (18)) with intensity ratio 5/21/25/49 with different linewidths. This simulation fits quite well with the three sites (OH, F)*n* assumed for fluorine occupancy from the X-ray diffraction analysis. In this situation, the weakest intensity peak could be considered as corresponding to an impurity. This result shows that the fluorine population is different for the three crystallographic sites (OH, F)*n*; the corresponding sites could be occupied by either fluorine atom or hydroxyl groups.

## 3. RESULTS

The structure of MIL-12 can be described as a new type of macroanionic sheet, $[Al_2(PO_4)(OH, F)_5]^{2-}$, perpendicular to the *a* axis. Preliminary solid-state $^{19}F$ NMR experiments show that fluorine and hydroxyl groups are disordered on the corresponding sites (OH, F)*n*. As shown on Fig. 5, the diprotonated amine lies between the inorganic layers.

The inorganic layer (see Fig. 6) is built up from trans chains of corner-sharing Al(2) octahedra running parallel to

**TABLE 2**
**X-Ray Powder Diffraction Pattern of $(C_3H_{12}N_2)Al_2PO_4(OH,F)_5$**

| $h$ | $k$ | $l$ | $2\theta_{obs}$ (°) | $2\theta_{calc}$ (°) | $d_{obs}$ (Å) | $I_{obs}$ |
|---|---|---|---|---|---|---|
| 1 | 0 | 0 | 8.147 | 8.128 | 10.84 | 100 |
| 0 | 0 | 1 | 14.769 | 14.758 | 5.99 | 14 |
| 1 | 1 | 0 | 15.033 | 15.024 | 5.89 | 77 |
| $\bar{1}$ | 0 | 1 | 15.449 | 15.442 | 5.73 | 18 |
| 2 | 0 | 0 | 16.310 | 16.297 | 5.43 | 5 |
| 1 | 0 | 1 | 18.200 | 18.189 | 4.870 | 11 |
| 0 | 1 | 1 | 19.457 | 19.460 | 4.558 | 1 |
| $\bar{2}$ | 0 | 1 | 19.843 | 19.830 | 4.471 | 1 |
| $\bar{1}$ | 1 | 1 | 19.990 | 19.988 | 4.438 | 1 |
| $\bar{2}$ | 1 | 0 | 20.670 | 20.661 | 4.294 | 9 |
| 1 | 1 | 1 | 22.211 | 22.197 | 3.999 | 2 |
| $\bar{2}$ | 1 | 1 | 23.575 | 23.571 | 3.771 | 23 |
| 2 | 0 | 1 | 24.093 | 24.082 | 3.691 | 36 |
| 3 | 0 | 0 | 24.557 | 24.550 | 3.622 | 1L |
| 0 | 2 | 0 | 25.390 | 25.385 | 3.505 | 13 |
| $\bar{3}$ | 0 | 1 | 26.186 | 26.180 | 3.400 | 2 |
| $\bar{1}$ | 2 | 0 | 26.701 | 26.696 | 3.336 | 6 |
| 2 | 1 | 1 | 27.264 | 27.275 | 3.268 | 1 |
| $\bar{3}$ | 1 | 0 | 27.698 | 27.692 | 3.218 | 7 |
| $\bar{3}$ | 1 | 1 | 29.158 | 29.158 | 3.060 | 18 |
| $\bar{1}$ | 0 | 2 | 29.323 | 29.324 | 3.043 | 1 |
| $\bar{1}$ | 2 | 1 | 29.849 | 29.848 | 2.991 | 28 |
| 2 | 2 | 0 | 30.316 | 30.315 | 2.946 | 21 |
| 3 | 0 | 1 | 31.169 | 31.152 | 2.867 | 9 |
| $\bar{2}$ | 0 | 2 | | 31.173 | | |
| $\bar{1}$ | 1 | 2 | 32.028 | 32.034 | 2.792 | 9 |
| $\bar{2}$ | 2 | 1 | | 32.419 | | |
| 1 | 0 | 2 | 32.436 | 32.422 | 2.758 | 3 |
| 0 | 1 | 2 | | 32.445 | | |
| $\bar{4}$ | 0 | 1 | 33.490 | 33.484 | 2.674 | 2 |
| 3 | 1 | 1 | 33.745 | 33.730 | 2.654 | 13 |
| $\bar{2}$ | 1 | 2 | | 33.750 | | |
| 1 | 1 | 2 | 34.919 | 34.917 | 2.567 | 7 |
| $\bar{3}$ | 0 | 2 | 34.996 | 34.990 | 2.562 | 2 |
| $\bar{4}$ | 1 | 0 | 35.386 | 35.398 | 2.535 | 2 |
| 3 | 2 | 0 | 35.598 | 35.606 | 2.520 | 5 |
| $\bar{4}$ | 1 | 1 | 35.899 | 35.914 | 2.4995 | 1L |
| $\bar{3}$ | 2 | 1 | 36.781 | 36.788 | 2.4416 | 1L |
| 2 | 0 | 2 | 36.857 | 36.859 | 2.4367 | 1L |
| $\bar{3}$ | 1 | 2 | 37.319 | 37.334 | 2.4076 | 2 |
| 4 | 0 | 1 | 38.865 | 38.872 | 2.3153 | 2 |
| 2 | 1 | 2 | 39.096 | 39.106 | 2.3022 | 1L |

*Note.* 1L, Lower than 1.

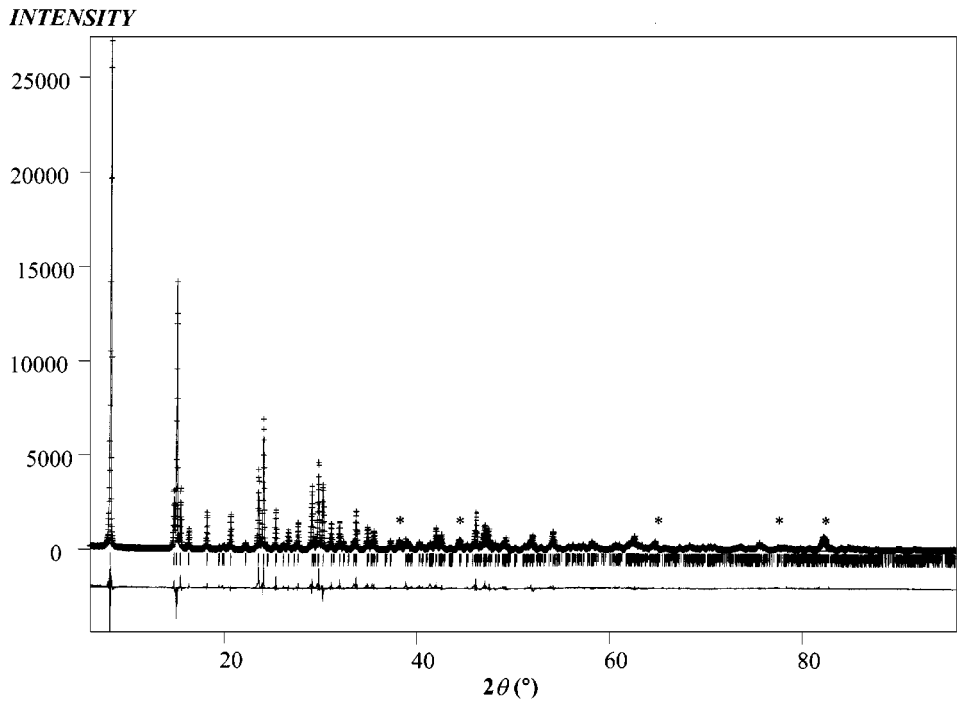


**FIG. 3.** Final Rietveld plot of $Al_2(PO_4)(OH_x, F_{5-x})N_2C_3H_{12}$. The observed data are shown by the crosses and the calculated data by the solid line; (*) denotes the excluded region corresponding to the spurious lines of the sample holder.

the *b* axis. Fluorine and hydroxyl groups ensure the connection of the octahedra along the chain. Satellites composed by an $Al(1)O_2(OH, F)_4$ octahedron and a $PO_4$ tetrahedron linked by corner are grafted to the chain in an alternated way (Figs. 6 and 8a). Aluminum octahedra then develop a double zig-zag chain along the *b* axis. They are connected by the phosphate groups to form the layer perpendicular to the *a* axis. The four corners of the phosphate group are shared to aluminum octahedra; three of them belong to the same octahedra chain and the fourth to the other chain.

**TABLE 3**
**Positional Parameters and Their Standard Deviations for $(C_3H_{12}N_2)Al_2PO_4(OH, F)_5$**

| Atom | *x* | *y* | *z* |
|---|---|---|---|
| P | 0.1656(4) | 0.25 | 0.2761(9) |
| Al(1) | 0.2595(5) | 0.25 | − 0.215(1) |
| Al(2) | 0 | 0 | 0.5 |
| O1 | 0.2279(9) | 0.25 | 0.080(2) |
| O2 | 0.0873(7) | 0.071(1) | 0.277(1) |
| O3 | 0.2714(9) | 0.25 | 0.502(2) |
| (OH, F) 1 | 0.9431(9) | 0.25 | 0.513(2) |
| (OH, F) 2 | 0.1309(6) | 0.0563(9) | − 0.286(1) |
| (OH, F) 3 | 0.3682(6) | 0.0607(9) | − 0.152(1) |
| N1 | 0.154(1) | − 0.25 | 0.060(2) |
| C1 | 0.292(1) | − 0.25 | 0.149(3) |
| C2 | 0.313(1) | − 0.25 | 0.414(3) |
| C3 | 0.454(1) | − 0.25 | 0.506(3) |
| N2 | 0.484(1) | − 0.25 | 0.742(2) |

*Note.* Overall isotropic temperature factor = 0.31(6) $Å^2$.

The layer could also be described in terms of structural units (see Fig. 7) formed with the two independent aluminum octahedra and the phosphate group. Al(1) and Al(2) are both surrounded by four fluorines or hydroxyls and 2 oxygen atoms of 2 phosphate groups which are in *trans* positions. The Al(2) octahedron shares all its vertices with other polyhedra while the Al(1) octahedron has two fluorines or hydroxyls in terminal position. In the aluminum octahedra, distances range from 1.76(1) to 1.955(8) Å for Al(1) and from 1.802(7) to 1.885(7) Å for Al(2) (see Table 4). The mean values (1.86(9) and 1.85(4) Å for Al(1) and Al(2), respectively) are in good agreement with those previously observed in similar compounds (12, 19). The P–O distances range from 1.49(1) to 1.63(1) Å with an average distance of 1.54(6) Å. Moreover, each Al(1) octahedron is connected to two phosphate groups by sharing its vertices in *trans* position and develops infinite chains along the *c* axis (Fig. 6). The connection between two structural units of two neighboring chains generates 6-polyhedron channels along the *a* axis. The connectivity between inorganic layers is ensured by the organic molecules via hydrogen bonds. The most probable hydrogen bonds are listed in Table 4. One of the ammonium of 1–3 Diaminopropane (N1), interacts

**TABLE 4**
**Selected Bond Distances (Å) and Angles (°) for $(C_3H_{12}N_2)Al_2PO_4(OH, F)_5$**

| | | | |
|---|---|---|---|
| | Within the $PO_4$ tetrahedron | | |
| P–O1 | 1.49(1) | O1–P–O2 | 110.6(9) |
| P–O2 | 1.523(8) | O1–P–O2$^a$ | 110.6(9) |
| P–O2$^a$ | 1.523(8) | O1–P–O3 | 108(1) |
| P–O3 | 1.63(1) | O2–P–O2$^a$ | 110.6(7) |
| | | O2–P–O3 | 108.4(9) |
| | | O2$^a$–P–O3$^a$ | 108.4(9) |
| | Within $AlO_6$ octahedra | | |
| Al1–O1 | 1.90(1) | Al1–(OH, F)2$^a$ | 1.955(8) |
| Al1–O3$^b$ | 1.76(1) | Al1–(OH, F)3 | 1.783(8) |
| Al1–(OH, F)2 | 1.955(8) | Al1–(OH, F)3$^a$ | 1.783(8) |
| O1–Al1–O3$^b$ | 174(1) | O3$^b$–Al1–(OH, F)3$^a$ | 92.2(7) |
| O1–Al1–(OH, F)2 | 87.3(6) | (OH, F)2–Al1–(OH, F)2$^a$ | 88.0(5) |
| O1–Al1–(OH, F)2$^a$ | 87.3(6) | (OH, F)2–Al1–(OH, F)3 | 87.9(5) |
| O1–Al1–(OH, F)3 | 92.0(7) | (OH, F)2–Al1–(OH, F)3$^a$ | 175.8(6) |
| O1–Al1–(OH, F)3$^a$ | 92.0(7) | (OH, F)2$^a$–Al1–(OH, F)3 | 175.8(6) |
| O3$^b$–Al1–(OH, F)2 | 88.3(6) | (OH, F)2$^a$–Al1–(OH, F)3$^a$ | 87.9(5) |
| O3$^b$–Al1–(OH, F)2 | 88.3(6) | (OH, F)3–Al1–(OH, F)3$^a$ | 96.2(5) |
| O3$^b$–Al1–(OH, F)3 | 92.2(7) | | |
| Al2–O2 | 1.885(7) | Al2–(OH, F)1$^e$ | 1.869(3) |
| Al2–O2$^c$ | 1.885(7) | Al2–(OH, F)2$^f$ | 1.802(7) |
| Al2–(OH, F)1$^d$ | 1.869(3) | Al2–(OH, F)2$^g$ | 1.802(7) |
| O2–Al2–O2$^c$ | 180.0(7) | O2$^c$–Al2–(OH, F)2$^g$ | 90.9(6) |
| O2–Al2–(OH, F)1$^d$ | 90.2(6) | (OH, F)1$^d$–Al2–(OH, F)1$^e$ | 180.0(3) |
| O2–Al2–(OH, F)1$^e$ | 89.8(5) | (OH, F)1$^d$–Al2–(OH, F)2$^f$ | 89.7(5) |
| O2–Al2–(OH, F)2$^f$ | 90.9(6) | (OH, F)1$^d$–Al2–(OH, F)2$^g$ | 90.3(5) |
| O2–Al2–(OH, F)2$^g$ | 89.1(5) | (OH, F)1$^e$–Al2–(OH, F)2$^f$ | 90.3(5) |
| O2$^c$–Al2–(OH, F)1$^d$ | 89.8(5) | (OH, F)1$^e$–Al2–(OH, F)2$^g$ | 89.7(5) |
| O2$^c$–Al2–(OH, F)1$^e$ | 90.2(6) | (OH, F)2$^f$–Al2–(OH, F)2$^g$ | 180.0(7) |
| O2$^c$–Al2–(OH, F)2$^f$ | 89.1(5) | | |
| | Within organic cation | | |
| N1–C1 | 1.52(2) | N1–C1–C2 | 108(2) |
| C1–C2 | 1.59(2) | C1–C2–C3 | 108(2) |
| C2–C3 | 1.55(2) | C2–C3–N2 | 113(2) |
| C3–N2 | 1.42(2) | | |
| | Most probable hydrogen bonds | | |
| N1...O2 | 2.78(1) | N2...(OH, F)3$^f$ | 2.67(1) |
| N1...O2$^h$ | 2.78(1) | N2...(OH, F)3$^i$ | 3.02(1) |
| N1...(OH, F)1$^i$ | 3.01(2) | N2...(OH, F)3$^j$ | 2.67(1) |
| N1...(OH, F)2 | 2.99(1) | N2...(OH, F)3$^k$ | 3.02(1) |
| N1...(OH, F)2$^h$ | 2.99(1) | | |

*Note*. Symmetry codes: (*a*) $x, \frac{1}{2}-y, z$; (*b*) $x, y, z-1$; (*c*) $-x, -y, 1-z$; (*d*) $x-1, y, z$; (*e*) $1-x, y-\frac{1}{2}, 1-z$; (*f*) $x, y, z+1$; (*g*) $-x, -y, -z$; (*h*) $x, -y-\frac{1}{2}, z$; (*i*) $1-x, y-\frac{1}{2}, 1-z$; (*j*) $x, -y-\frac{1}{2}, z+1$; (*k*) $1-x, -y, 1-z$.

indifferently with the oxygens of $PO_4$ groups and with the bridging (OH, F) groups, while the other (N2) interacts only with the terminal (OH, F) groups. The shortest distances are: N1–O2 = 2.78 Å and N2–(OH, F)3$^f$ = 2.67 Å.

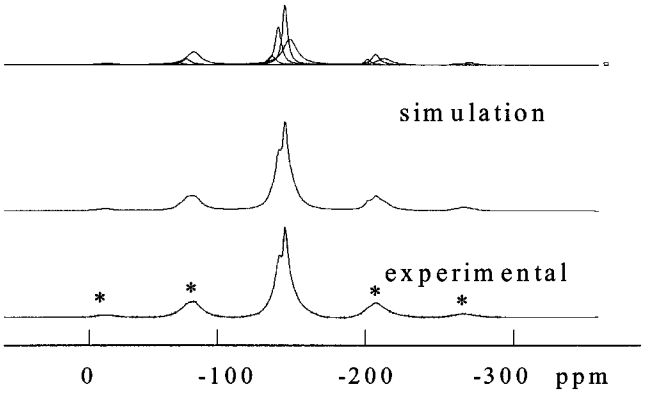


**FIG. 4.** $^{19}F$ MAS NMR spectrum (470.6 MHz, 30 kHz) of $Al_2(PO_4)(OH_x, F_{5-x})N_2C_3H_{12}$ (MIL-12); (*) indicates spinning sidebands.

It can be noted that this kind of Al(2) octahedra chain has already been found in some natural and synthetic aluminophosphates. For example, in the mineral Tancoïte, $LiNa_2HAl(PO_4)_2(OH)$ (20), and in the one-dimensional aluminophosphate, $Na_4Al(PO_4)_2(OH)$ (19), described by Attfield *et al.*, the aluminum octahedra of these chains are surrounded by four phosphate groups (see Fig. 8b). A compound with the same Al/P ratio as MIL-12, formulated as $K_3[Al_4F_9(PO_4)_2]$, was also synthesized by Massa *et al.* (21). Its structure exhibits the same type of chain (Fig. 8c) and every aluminum octahedron of the chain is surrounded by two aluminum octahedra and two phosphate groups as in MIL-12, but instead of being on both sides of the chain, the two aluminum octahedra are located on the same side of the

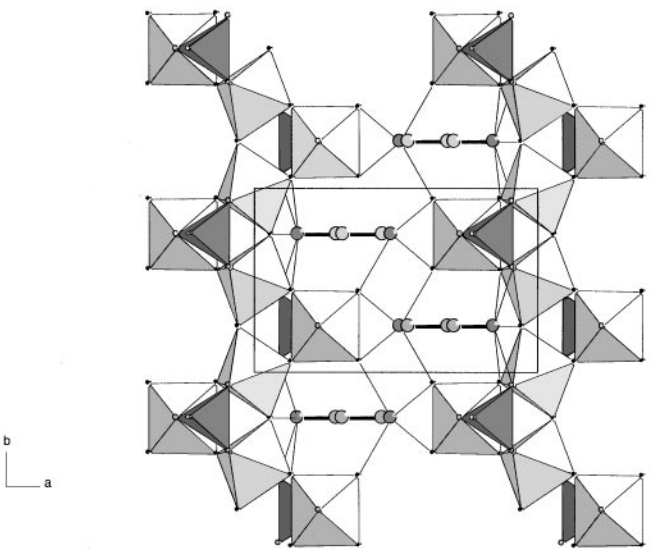


**FIG. 5.** View of MIL-12 along the [001] direction. Hydrogen bonds are shown as thin lines.

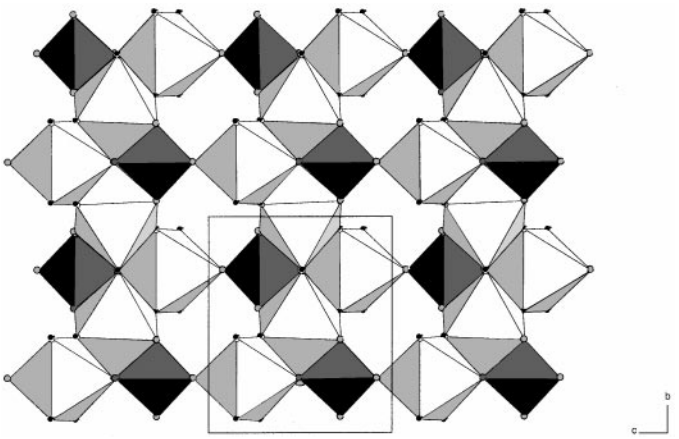

**FIG. 6.** View of the macroanionic sheet along the [100] direction.

chain and the two phosphate groups are located on the other side. The connection between the two types of polyhedra satellites ensured a three-dimensional network.

## 4. DISCUSSION

Recently, Ozin *et al.* (22) proposed a new model for aluminophosphate formation starting from a parent chain of corner-sharing Al and P tetrahedra in strict alternation, which can give rise to a family of solids with various dimensionalities. The P : Al ratio of this chain was 2. The chain described here is totally different with Al in octahedral coordination and Al–O–Al linkage. It presents also a large

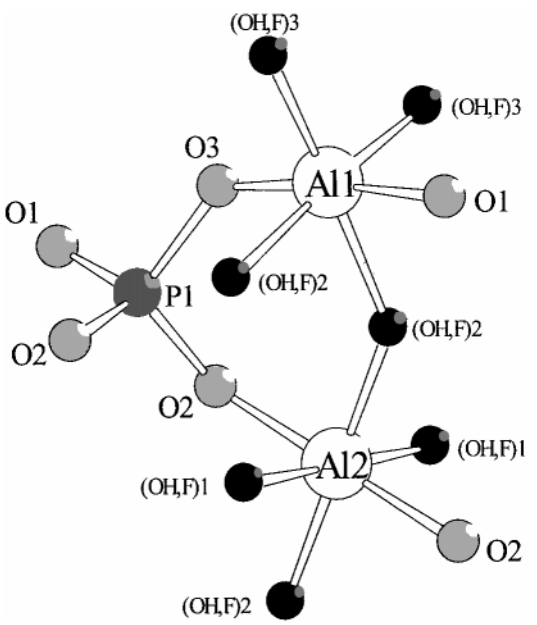


**FIG. 7.** Stick and ball model of the structural unit.

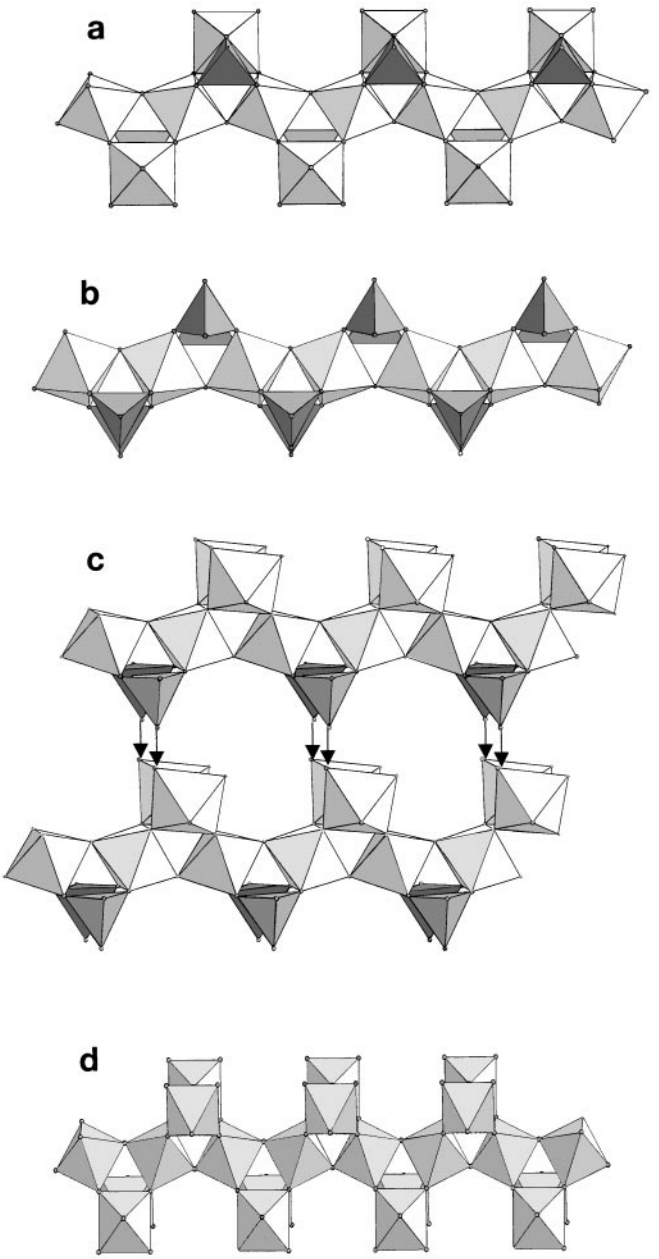


**FIG. 8.** Comparison of aluminum octahedra chains and their satellites in (a) MIL-12, (b) Tancoïte, (c) $K_3[Al_4F_9(PO_4)_2]$, and (d) $AlF_3$.

variability of compositions ($1/2 < P/Al < 2$) and topologies, based on the nature and the relative position of the polyhedra grafted on the invariant central *trans* chain of corner sharing Al octahedra.

This chain can be written $[Al_{2-x}P_x][Al_2][Al_{2-y}P_y]$ in a general way, indicating the nature of the cations on the left and the right side of the central Al chain. $x = y = 2$ corresponds to the tancoïte chain and $x = y = 1$ describes the title compound, whereas $x = 2$, $y = 0$ relates to Massa's compound. The organization of the chains determines the

dimensionality of the structure. In the first compound, the central chain being shielded by exclusively external $PO_4$ tetrahedra prevents from any further connection to another chain and explains the 1D character of the solid. In the second, the mixed character on both sides allows the formation of a second chain orthogonal to the central chain and therefore a layered solid, but the relative disposition of the satellites chains rules out connection in the third direction. Finally, the segregation of Al and P on each side of the chain, and the topological relation between the isolated $PO_4$ tetrahedron and the Al–Al chain on the other side permits the grafting between the satellite moieties of two consecutive chains. The other limit of the series, with only grafted Al octahedra ($x = y = 0$) is obviously not an aluminum phosphate, but exists in the pyrochlore form of $FeF_3$, $CrF_3$, and $AlF_3$ (23) (Fig. 8d).

## REFERENCES


1. S. T Wilson, B. M. Lok, C. A. Messina, and E. M. Flanigen, *J. Am. Chem. Soc*. **104,** 1146 (1982).
2. J. L. Guth, H. Kessler, and R. Wey, *Stud. Surf. Sci. Catal.* **28,** 121 (1986).
3. T. Loiseau and G. Férey, *J. Chem. Soc., Chem. Commun.* 1197 (1992).
4. D. Riou, T. Loiseau, and G. Férey, *J. Solid State Chem.* **102,** 4 (1993).
5. M. Cavellec, D. Riou, C. Ninclaus, J.M. Grenèche, and G. Férey, *Zeolites* **17,** 250 (1996).
6. D. Riou and G. Férey, *J. Solid State Chem.* **111,** 422 (1994).
7. C. Serre and G. Férey, *J. Mater. Chem.* **9,** 579 (1999).
8. G. Férey, *J. Fluorine Chem.* **73,** 187 (1995); C. R. *Acad Sci. Paris*, **1,** Série II *c*, 1–13 (1998).
9. M. Cavellec, D. Riou, and G. Férey, *Eur. J. Solid State Inorg. Chem.* **31,** 583 (1994).
10. T. Loiseau, F. Taulelle, and G. Férey, *Microporous Mater*. **9,** 83 (1997).
11. M. Cavellec, C. Egger, J. Linares, M. Nogues, F. Varret, and G. Férey, *J. Solid State Chem.* **134,** 349 (1997).
12. N. Simon, T. Loiseau, F. Taulelle, and G. Férey, *Chem. Mater*., submitted.
13. A. Boultif and D. Louër, *J. Appl. Crystallogr*. **24,** 987 (1991).
14. A. D. Mighell, C. R. Hubbard, and J. K. Stalik. . [NBS*AIDS80: A Fortran Program for Crystallographic Data Evaluation. Nat. Bur. Stand. (U.S.). Technical Note No. 1141, 1981. [NBS*AIDS83 is an expanded version of NBS*AIDS80].
15. J. Rodriguez-Carvajal, in "Collected Abstracts of Powder Diffraction Meeting", p. 127. Toulouse, France 1990.
16. A. Altomare, M. C. Burla, M. Camalli, G. Cascarano, C. Giacovazzo, A. Guagliardi, and G. Polidori, *J. Appl. Cryst*. **27,** 435 (1994).
17. F. Taulelle, T. Loiseau, J. Maquet, J. Livage, and G. Férey, *J. Solid State Chem.* **105,** 191 (1993).
18. Winfit/WinNMR, Bruker Program Simulation.
19. M. P. Attfield, R. E. Morris, I. Burshtein, C. F. Campana, and A. K. Cheetham, *J. Solid State Chem.* **118,** 412 (1995).
20. R. A. Ramik, B. D. Sturman, P. J. Dunn, and A. S. Poverennykh, *Can. Miner*. **18,** 185 (1980).
21. W. Massa, O. V. Yakubovich, O. V. Karimova, and L. N. Dem'yanets, *Acta Crystallogr. Sect. C* **51,** 1246 (1995).
22. S. Olivier, A. Kuperman, and G. A. Ozin, *Angew. Chem. Int. Ed*. **37,** 46 (1998).
23. R. de Pape and G. Férey, *Mater. Res. Bull.* **21,** 971 (1986).